Highly Efficient Photoninitiators Based on 4H-Pyranylidene Derivatives for Two-Photon Laser Printing

ADVANCED MATERIALS TECHNOLOGIES
www.advmattechnol.de

Highly Efficient Photoninitiators Based on 4*H*-Pyranylidene Derivatives for Two-Photon Laser Printing

Raquel Royo, Philipp Mainik, Carlos Benitez-Martin, Raquel Andreu, Eva Blasco,* Francisco Najera,* and Belén Villacampa*

A series of four donor–acceptor–donor derivatives bearing 4*H*-pyranylidene and 4-methylcyclohexan-1-one units as donor and acceptor groups respectively is designed, synthesized, and photophysically characterized. Both experimental and theoretical studies reveal good two-photon absorption (2PA) properties for these systems. Decoration of the exocyclic position of the 4*H*-pyranylidene moiety with a thiophene ring results in high 2PA cross-section values (σ_{2PA}) ≈700 nm, and remarkably, in the region between 900 and 1000 nm. Furthermore, all chromophores are evaluated as photoinitiators (PIs) for two-photon-laser printing at 780 nm, showing superior performance compared to the commonly used commercially available PI, phenylbis(2,4,6-trimethylbenzoyl)phosphine oxide. Among the studied PIs, the ones equipped with a thiophene unit at the exocyclic position of the 4*H*-pyranylidene moiety exhibit the highest efficiency, enabling fast printing using low laser powers with even lower concentrations of PI. Overall, this study shows the great potential of this new class of PIs for application in the field of 3D nanoprinting.

1. Introduction

Two-photon laser printing (2PLP), also known as 3D direct laser writing or 3D nanoprinting, is a solid free-form fabrication technique where a resin, containing both a multifunctional monomer and a photoinitiator (PI), is cured at the focal spot of a pulsed near-infrared laser. 2PLP has aroused great interest in the last years for applications requiring 3D structures with high spatial resolution.[1,2]

In this context, two-photon absorption (2PA) active PIs play a paramount role to obtain efficient and spatially controlled polymerization, leading to high-quality structures. With 2PA being a third-order nonlinear optical (NLO) phenomenon, its rate depends quadratically on the light intensity.[3] Most applications making use of 2PA processes, such as 3D microfabrication or nonlinear imaging microscopy, build on this intensity dependence. The 2PA cross section (σ_{2PA}) is the parameter commonly used to quantify the nonlinear absorption ability. Similar to the molar extinction coefficient (ϵ) for one-photon absorption, the σ_{2PA} value accounts for the probability of reaching an excited state but does not give any information on subsequent photochemistry. Therefore, a high σ_{2PA} is not the only criterion for a PI to show good performance in 2PLP. Other essential requirements are the solubility, stability, and initiation efficiency of the PI and its excited states in the

R. Royo, R. Andreu
Instituto de Nanociencia y Materiales de Aragón (INMA)-Departamento de Química Orgánica
CSIC-Universidad de Zaragoza
Zaragoza 50009, Spain
E-mail: randreu@unizar.es

P. Mainik, E. Blasco
Institute for Molecular Systems Engineering and Advanced Materials (IMSEAM)
Heidelberg University
im Neuenheimer Feld 225, 69120 Heidelberg, Germany
E-mail: eva.blasco@oci.uni-heidelberg.de

C. Benitez-Martin
Department of Chemistry and Chemical Engineering
Chalmers University of Technology
Gothenburg 41296, Sweden

F. Najera
Departamento de Química Orgánica
Universidad de Málaga
Campus Teatinos s/n, Málaga 29071, Spain
E-mail: najera@uma.es

F. Najera
Instituto de Investigación Biomédica de Málaga y Plataforma en Nanomedicina–IBIMA
Plataforma Bionand, Parque Tecnológico de Andalucía
Málaga 29590, Spain

B. Villacampa
Instituto de Nanociencia y Materiales de Aragón (INMA)-Departamento de Física de la Materia Condensada
CSIC-Universidad de Zaragoza
Zaragoza 50009, Spain

The ORCID identification number(s) for the author(s) of this article can be found under https://doi.org/10.1002/admt.202300571

DOI: 10.1002/admt.202300571

monomer composition.[1] Moreover, low fluorescence quantum yields are usually desired as this leads to a higher population of the active state for initiating the polymerization.[4,5]

Rational design strategies for 2PLP PIs have allowed for great advances in the last 20 years,[6,7] paving the way for efficient 2PLP. Following one of these strategies, powerful 2PA chromophores have been designed and evaluated[7,8] by combining strong donor (D) and acceptor (A). Among them, symmetric quadrupolar chromophores with two donor moieties and an electron-withdrawing core (D–π–A–π–D) have been found to have high σ_{2PA} values in combination with good initiating efficiency.[9–11] As regards to donor groups, dialkylaminoanilines[10,12–14] together with triarylamines[15,16] have been extensively studied.

Concerning the π-spacer, there are two main parameters directly affecting the 2PA properties: 1) the rigidity, and 2) the size or length, often represented by the number of π-electrons provided to the electronic system. Among the different alternatives that have been thoroughly studied,[3] the incorporation of aromatic heterocycles, such as thiophene, has given rise to extended π-conjugated systems, yielding materials with high σ_{2PA}.[16] Indeed, the use of this heterocycle fulfills the previous criteria, as it provides a considerable number of electrons to the π-relay within a rigid and condensed structural unit.

Finally, looking for low fluorescence materials, carbonyl moieties[9,11,17,18] and recently triazine moieties[19] have been explored as good electronic acceptors.

Despite the significant progress in the design of 2PA active photoinitiators,[6,7] the availability of efficient systems for 2PLP is still limited.[7] To promote two-photon 3D printing into the market, the development of efficient two-photon PIs is highly desirable to guarantee fast printing rates, and, finally, to address structures with a high resolution.[13]

The 4*H*-pyranylidene moiety is a proaromatic electron-donating unit that gains aromaticity on charge transfer.[20] Due to this promoted donor ability, it is a building block often used in the design of π-conjugated systems in different areas, like second-order NLO applications[21] or dye-sensitized solar cells.[22]

In this context, and taking advantage of our consolidated experience in D–π–A systems with the 4*H*-pyranylidene as a donor unit,[20,23–26] in the present work, its excellent donor ability has been applied in the design of derivatives with a D–A–D structure as 2PLP PIs. The novelty of using the pyran moiety as a donor unit for the application in 2PLP is worth noting. 2PA activity has been reported for some pyran derivatives[27,28] featuring mainly this moiety as π-spacer[29] but, the potential of this donor moiety as 2PLP PIs has, to the best of our knowledge, not been investigated before.

Thus, we present the synthesis, optical characterization, and photoinitiation potential in 2PLP of the series of molecules shown in **Figure 1**. Chromophores were built according to the following approach: i) the novelty of using the pyran moiety as a donor unit for 2PLP PIs; ii) the good results achieved with a carbonyl group used as acceptor unit, and iii) the incorporation of aromatic heterocycles (namely thiophene) in the π-relay. Two structural variations (R_1 and R_2 groups) are proposed and studied.

The linear and nonlinear optical properties of the chromophores were investigated by means of spectroscopic techniques and quantum chemical methods. Finally, the photoinitiation ability of these systems was evaluated in a series of 2PLP experiments.

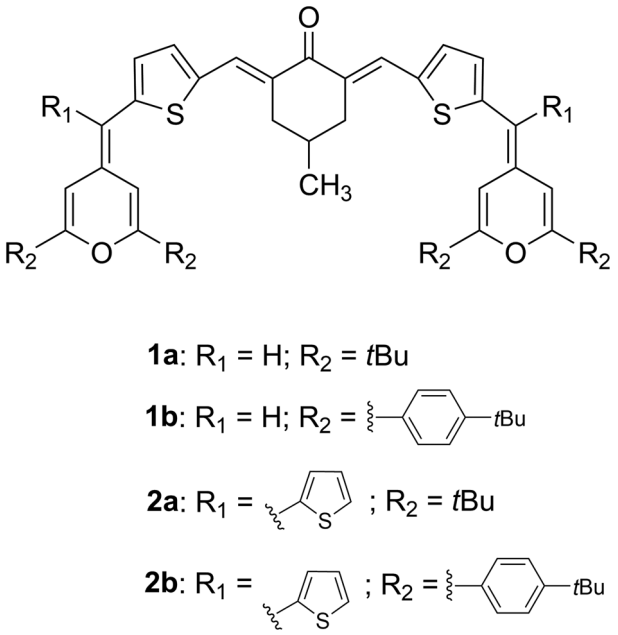

Figure 1. Chemical structures of the photoinitiators under study.

2. Results and Discussion

2.1. Synthesis

Compounds **1a–b** and **2a–b** (Figure 1) were prepared from our previously reported aldehydes **3a**,[30] **3b**,[31] and **4a**,[26] as well as the novel **4b** (**Figure 2**).

Aldehyde **4b** was synthesized in overall good yield by following a methodology similar to that used to obtain analog **4a**,[26] which consists of two steps as represented in **Scheme 1**. First, intermediate **7** was obtained by a Wittig reaction between tributylphosphonium perchlorate **5**[31] and commercially available

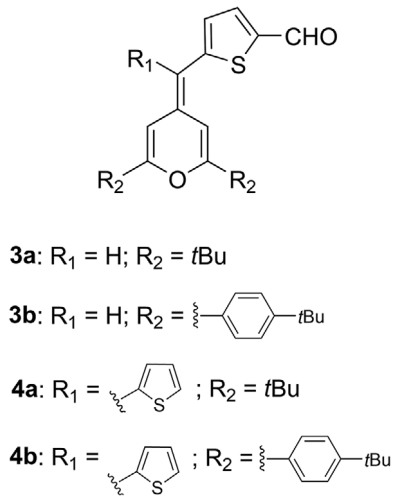

Figure 2. Precursor aldehydes.

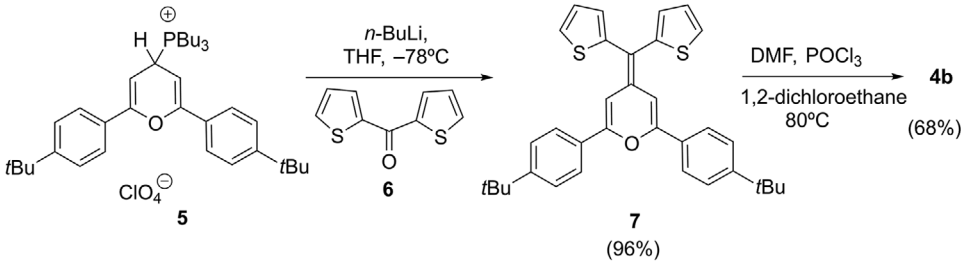

Scheme 1. Synthesis of aldehyde **4b**.

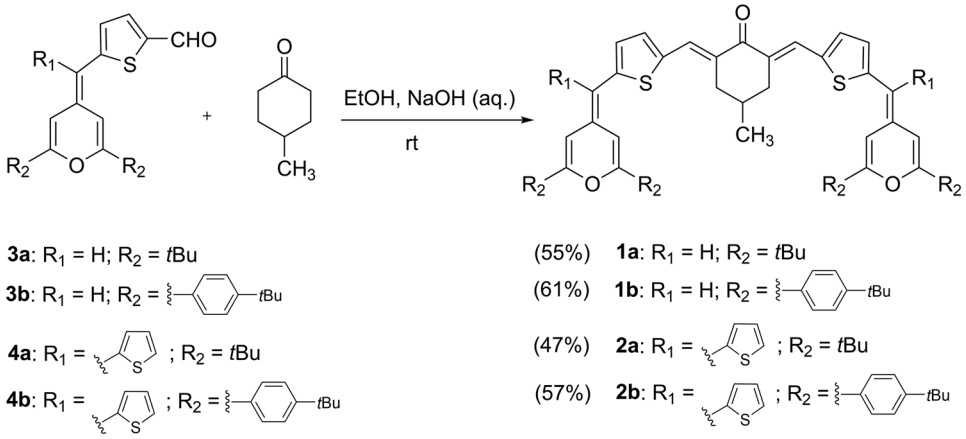

Scheme 2. Synthesis of chromophores **1a–b** and **2a–b**.

dithienylketone **6**. Subsequent formylation of **7** under classical Vilsmeier–Haack conditions resulted in the desired **4b**.

Photoinitiators **1a–b** and **2a–b** were afforded (**Scheme 2**) by Knoevenagel condensation between commercially available 4-methylcyclohexan-1-one and the previously prepared aldehydes (2 equiv.) (Figure 2) in ethanol, with yields ranging from 47% to 61%.

Reactions were monitored by TLC, and more portions of aqueous sodium hydroxide were added during the reaction time until the completion of the starting materials. Compounds **1a–b** and **2a–b** were eventually isolated by filtration, and purified by trituration with cold mixtures of solvents (more details are provided in the Experimental Section).

Regarding the configuration of the newly formed C=CH bond, the observed chemical shift indicates that these derivatives present an *E* configuration. More specifically, this proton signal is in all cases ≈7.90 ppm, due to the deshielding effect induced by the adjacent carbonyl group.[9]

2.2. Optical Properties

The photophysical properties of compounds **1a–b** and **2a–b** were investigated by UV/Vis absorption and fluorescence spectroscopy in two representative solvents, namely toluene and dichloromethane (data and spectra in toluene are summarized in **Table 1** and **Figure 3**; those in dichloromethane are shown in the Table S1, Supporting Information).

All PIs are characterized by broad and intense absorption bands in toluene with maxima in the green spectral region

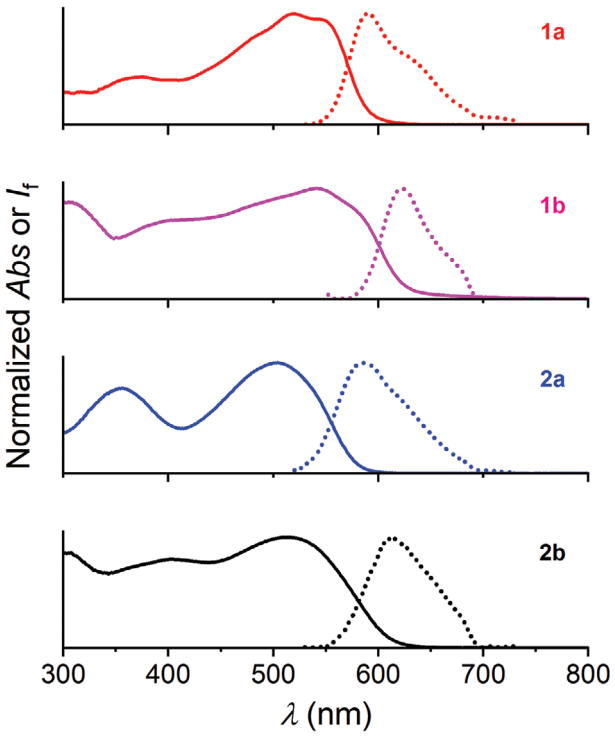

Figure 3. UV/Vis absorption (solid lines) and fluorescence spectra (dashed lines) of compounds **1a–b** and **2a–b** in toluene (≈10^{-5} M, air-equilibrated solutions).

Table 1. UV/Vis absorption and emission data in toluene (≈10^{-5} M, air-equilibrated solutions).

Compound	λ_{abs} [nm][a]	ϵ [M^{-1} cm^{-1}]	λ_{em} [nm][b]	Stokes shift [cm^{-1}][c]	Φ_{fl}[d]	$\lambda_{abs,2P}$ (nm)[e] [σ_{2PA} (GM)][f]	$\lambda_{em,2P}$ [nm][g]
1a	521	39 300	590	2245	0.071	700 [46]	600
1b	542	28 300	623	2399	0.013	700 [70]	630
2a	506	43 500	585	2669	0.003	700 [2497] 950 [649] 980 [639]	585
2b	515	33 300	614	3131	0.001	710 [1863] 950 [556] 980 [362]	612

[a] Lowest-energy electronic absorption maxima; [b] Fluorescence emission maxima; [c] Stokes shift as the difference (in wavenumber units) between the emission and absorption maxima; [d] Fluorescence emission quantum yield, ≈10% error; [e] Maxima from the 2PA spectra; [f] 2PA cross-section values determined by the 2PIF method, ≈15% error. [g] Fluorescence maxima under two-photon excitation at the maximum of the corresponding 2PA spectra.

Table 2. Calculated electronic and photophysical data for photoinitiators **1a** to **2b** at PCM (toluene)/M062X/6-31G(d) level.

Compound	Transition[a]	f[b]	Dominant component [%][c]	E_{calc} [eV][d]	$Emax_{exp}$ [eV][e]
1a	$S_0 \rightarrow S_1$	1.539	HOMO → LUMO (84) HOMO − 1 → LUMO + 1 (12)	2.61	2.38
	$S_0 \rightarrow S_2$	0.819	HOMO − 1 → LUMO (80) HOMO → LUMO + 1 (17)	2.99	
1b	$S_0 \rightarrow S_1$	1.497	HOMO → LUMO (81) HOMO − 1 → LUMO + 1 (14)	2.49	2.29
	$S_0 \rightarrow S_2$	1.271	HOMO − 1 → LUMO (74) HOMO → LUMO + 1 (23)	2.85	
2a	$S_0 \rightarrow S_1$	1.268	HOMO → LUMO (81) HOMO − 1 → LUMO + 1 (13)	2.71	2.45
	$S_0 \rightarrow S_2$	0.619	HOMO − 1 → LUMO (77) HOMO → LUMO + 1 (19)	3.00	
2b	$S_0 \rightarrow S_1$	1.050	HOMO → LUMO (77) HOMO − 1 → LUMO + 1 (16)	2.60	2.41
	$S_0 \rightarrow S_2$	1.170	HOMO − 1 → LUMO (69) HOMO → LUMO + 1 (25)	2.87	

[a] Corresponding to the $S_0 \rightarrow S_1$ and $S_0 \rightarrow S_2$ absorption transitions; [b] Oscillator strength; [c] Percentage of the contribution approximated by $2ci^2 \times 100\%$; [d] Calculated energies values determined in toluene; [e] Experimental values of the lowest energy maxima in toluene.

(Figure 3). According to time-dependent density functional theory calculations at two different levels of theory (i.e., CAM-B3LYP/6-31G(d) and M062X/6-31G(d), considering also solvent effects by including polarizable continuum medium (PCM)), these bands result from the overlap between $S_0 \rightarrow S_1$ and $S_0 \rightarrow S_2$ transitions (See **Table 2** and more details available in the Tables S2–S4, Supporting Information).

Delving deeper into these transitions, both are intricate and involve multiple one-electron excitations according to the natural transition orbitals (NTOs) analysis (see Table S5, Supporting Information). The $S_0 \rightarrow S_1$ combines HOMO→LUMO and HOMO − 1→LUMO + 1 transitions, whereas $S_0 \rightarrow S_2$ implies HOMO − 1→LUMO and HOMO→LUMO + 1 ones. Additionally, the fact that HOMO and HOMO − 1 are distributed over the arms of these molecules together with that LUMO and LUMO + 1 are centered over the central unit, suggests an intramolecular charge transfer (ICT) character for these transitions. A better understanding of this behavior is given by the corresponding electron density difference plots (See Tables S6, S7, Supporting Information), where the ICT character is clearly

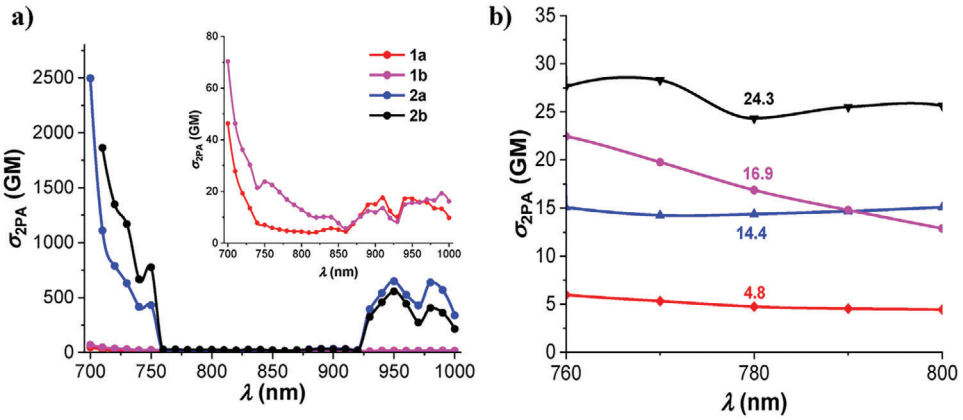

Figure 4. a) 2PA spectra of dyes **1a–b** and **2a–b**. The inset amplifies the 2PA spectra of **1a** and **1b** for better visualization; b) Zoom-in of the 2PA cross-sections of the dyes at 780 nm, the wavelength used for the 2PLP process.

detected as significant electron density shifts are drawn from the donor groups to the central acceptor moiety in both electronic transitions.

Noteworthy, the results obtained at both levels of theory are comparable and consistent with the experimental behavior.

In relation to the trends in the absorption energy values, these are directly related to the effective conjugation along the chromophores and are ultimately dictated by the structural composition. In this regard, two different effects are noted. On one hand, the presence of the thiophene moiety as R_1 in series **2** (see Figure 1), nearly orthogonal to the extended π-system,[26,32] imposes a slight deviation from planarity when compared with compound **1**. This fact translates into less efficient conjugation and subsequent hypsochromic shifts in the absorption of series **2**. This observation is in agreement with the behavior of recently reported compounds devised as donor materials for organic photovoltaics[32] or second-order NLO-phores.[33] On the other hand, and associated with the influence of substituents at positions 2 and 6 of the pyranylidene ring (R_2, see Figure 1), the more extended conjugated systems in compounds of series **b** (with R_2 = 4-*tert*-butylphenyl) lead to a red shift of λ_{max} versus those of series **a**, this being even more pronounced in derivatives **1**.

Additionally, systems **2** presented higher molar extinction coefficients (ϵ) than those of analogs **1**.

Akin to the absorption spectra, broad and structureless bands, with maxima between 585 and 623 nm, are observed in the fluorescence spectra. Their relative spectral position is also conducted by the structural differences, and, a similar reasoning as for the absorption bands can be applied. Accordingly, compounds of series **1** have red-shifted emissions compared to those of series **2** (Table 1), and within each series, analogs **b** emit at larger wavelength. In addition, these compounds show increased Stokes shifts from **1a** to **2b**, varying between 2245 and 3131 cm^{-1}. The fluorescence quantum yields are low and attend to the energy gap law in photochemistry,[34] as the nonradiative deactivation pathways are more competitive for the lower energy emissive states (Table 1). In general, low fluorescence quantum yields are preferred for chromophores designed to act as PIs in 2P polymerization.[7]

2.3. Two-Photon Absorption Properties

The 2PA properties of these compounds in toluene between 700 and 1000 nm were explored by the two-photon-induced fluorescence (2PIF) method.[35] The data are summarized in Table 1, and the complete 2P-excitation and 2PIF emission spectra can be found in Figure S2 (Supporting Information).

The 2PA spectra of these derivatives are shown in **Figure 4**, where a large difference is observed between the two-photon cross-section (σ_{2PA}) values of compounds of series **1** and **2**. Although all compounds under study displayed similar 2PA spectra in terms of shape, dyes **2** showed high σ_{2PA} (2497 GM at 700 nm and 1863 GM at 710 nm, for **2a** and **2b** respectively), and interestingly, significant ones at 950 and 980 nm. Conversely, compounds belonging to series **1** exhibit considerably lower σ_{2PA} values in the whole spectral range (Figure 4). It is worth noting that in all cases there is two-photon absorption at 780 nm, that is, the wavelength used for the 2PLP process.

The biphotonic nature of the excitation in all cases is ensured by the observed quadratic dependence of the emission intensity on the laser excitation power (Figure S3, Supporting Information), and the fluorescence spectra acquired under these conditions resembled also those acquired under conventional excitation (see Table 1). This last fact proves that the same electronic states are involved in the emission process without relying on the excitation process mechanism or the excited state reached.

To further explore the performance of these compounds, additional computational calculations were carried out. These studies based on the 2PA process do not provide accurate σ_{2PA} values but are very useful to elucidate trends in the 2PA of these molecules (see Table S7, Supporting Information). These calculations showed that under two-photon excitation conditions, as anticipated for other analog symmetrical molecules,[36] the transition to the first excited state has a very low cross-section value. Instead, biphotonic excitation is only allowed when accessing higher electronic excited states, as discussed later.

As an illustrative example, the analysis of the 1PA and 2P-excitation spectra of **2a** is shown in **Figure 5** (the corresponding analysis on **2b** and **1a–b** is detailed in Figure S1, Supporting Information).

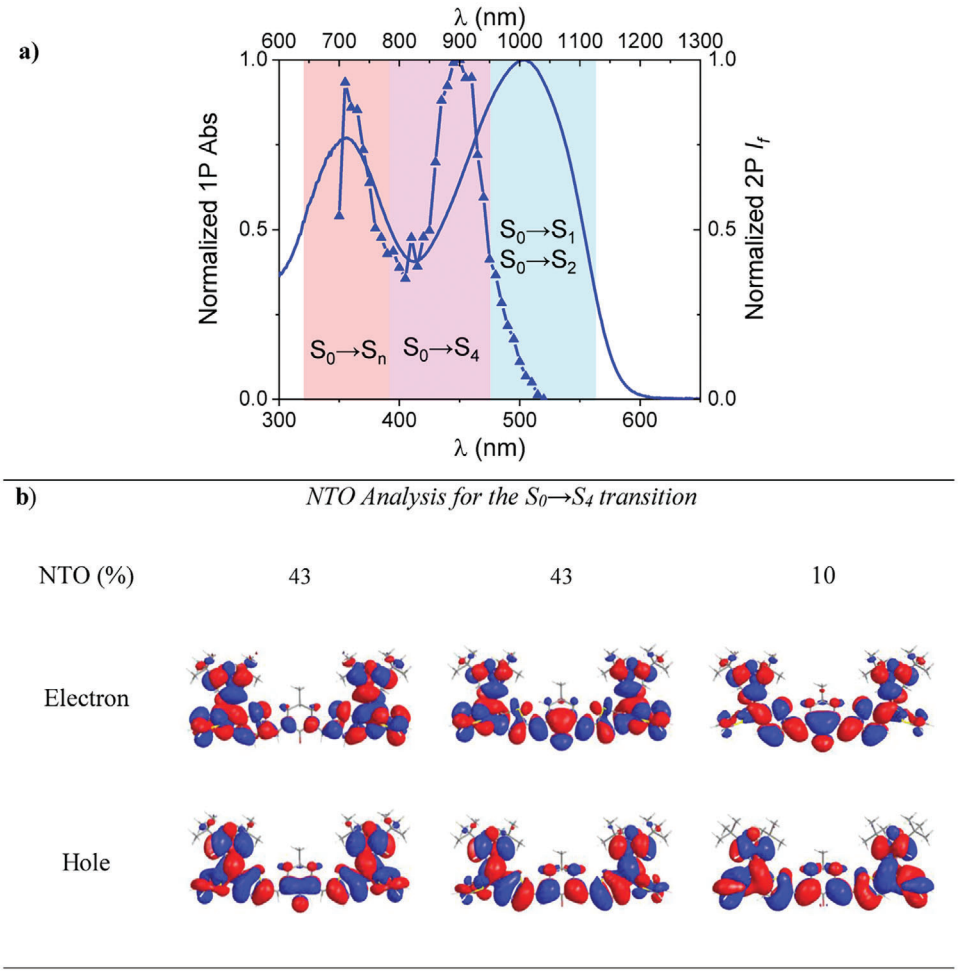

Figure 5. a) Comparison between 1PA (solid line) and 2P-excitation (solid line+triangles) spectra of **2a**, and assignment of the main electronic transitions; b) NTOs for transitions from the ground state to the fourth excited states in compound **2a**. The contributions of the NTOs to the respective transitions are indicated for each case. (Isosurface: 0.01 e bohr^{-3}).

As abovementioned, it is important to note that $S_0 \rightarrow S_1$ and $S_0 \rightarrow S_2$ transitions are close in energies and have high oscillator strength values under 1P conditions. These transitions are included under the band marked in blue for **2a**. Even if the transition to the first excited state is practically forbidden under two-photon excitation, the transition to the second one is relatively allowed. This explains the small shoulder observed at ≈960 nm in both cases. However, according to the 2P-calculations, the $S_0 \rightarrow S_4$ transition (highlighted in purple), is expected to exhibit a much greater σ_{2PA} versus that of $S_0 \rightarrow S_2$. Indeed, this is observed in Figure 5, where the most active transition involves the higher excited state. These observations can be extended to **2b,** although in this case, the $S_0 \rightarrow S_6$ transition is the most prominent 2P-active transition (see Figure S1, Supporting Information). Transitions to higher excited states with important σ_{2PA} are also predicted, being these appreciated at shorter wavelengths (marked in orange). On the other hand, compounds of series **1** display a similar behavior (Table S8, Supporting Information).

The NTOs analysis of compounds **2**, which are a proportional combination of the different elementary orbitals that participate in an electronic transition,[37] is described in Figures 5 and S1 for $S_0 \rightarrow S_4$ and for $S_0 \rightarrow S_6$ transitions for **2a** and **2b** respectively. In both NTOs analysis, the extra thienyl moieties incorporated into these compounds (in the exocyclic C=C of the pyranylidene unit) have an appreciable electronic density in the NTO-Hole, which could assist electronically to the NTO-Electron favoring the ICT along the Donor–Acceptor systems.

2.4. Photoinitiation in Two-Photon Laser Printing (2PLP)

Exploring the two-photon absorption properties of **1a–b** and **2a–b** was followed by a study on the photoinitiation ability in 2PLP, using a commercially available set-up with a laser wavelength of 780 nm. For this purpose, **1** and **2** were dissolved in pentaerythritol triacrylate (PETA) as crosslinker by ultrasonication for 3 h while heating to 55 °C to ensure complete dispersion of the PIs. The printability of the homogeneous photoresists with **1** and **2** in 2PLP was carefully investigated by varying the laser power between 5 and 15 mW and the scanning speeds between 2 and 20 mm s^{-1}. The quality of the printed 3D microstructures was evaluated by scanning electron microscopy (SEM). SEM

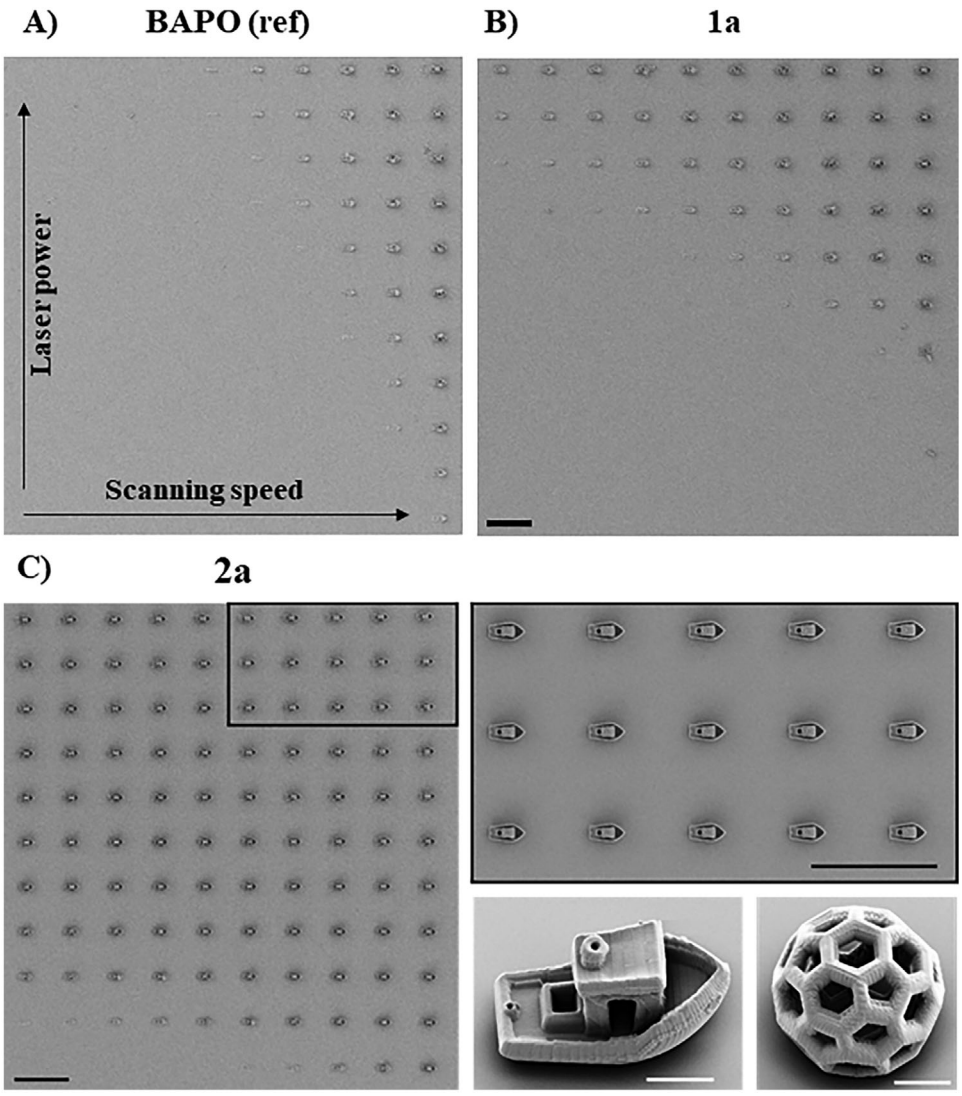

Figure 6. A) SEM image of the array with benchmark structures printed by 2PLP of PETA photoresist with BAPO as reference photoinitiator. The printing parameters were varied between 15 to 25 mW laser power in 1.0 mW increments (bottom–top) and 2 to 20 mm s^{-1} scanning speed in 2 mm s^{-1} steps (right–left). B),C) SEM image of the array with benchmark structures printed by 2PLP of PETA photoresists with new photoinitiators **1a** in (B) and **2a** in (C). The printing parameters were varied in both cases between 5 to 15 mW laser power in 1.0 mW increments (bottom–op) and 2 to 20 mm s^{-1} scanning speed in 2 mm s^{-1} steps (right–eft) The black rectangle in (C) shows a zoomed region with a laser power of 13 to 15 mW in 1.0 mW steps (bottom–op) and scanning speed of 2 to 10 mm s^{-1} in 2 mm s^{-1} increments. Furthermore, an SEM image of a printed benchmark and Buckminsterfullerene-like structure with **2a** using a laser power of 15 mW and scanning speed of 2 mm s^{-1} is shown in (C). The black and white scale bars are 100 and 10 µm, respectively.

images of the array with printed benchmark structures with **1a–b**, **2a–b**, and phenylbis(2,4,6-trimethylbenzoyl)phosphine oxide (BAPO) as photoinitiators are shown in **Figure 6** (and S4). BAPO is a commercially available PI commonly used in formulation for 2PLP and here used as a reference.[38–41] Comparing the printing parameters of the 3D printed microstructures using the chromophores with the reference photoresist containing BAPO reveal the significantly higher efficiency of **1a–b** and **2a–b** (**Table 3**).

First, the employed molar concentration of **1a–b** and **2a–b** was significantly lower (37 µmol g^{-1}) than BAPO (120 µmol g^{-1}) to achieve stable microstructures by 2PLP.[38] In addition, even at the 3.3 times lower molar concentration, photoresists with **1** and **2** could be photopolymerized with significantly lower laser powers than the BAPO photoresist while maintaining the same scanning speed. The 2PLP printed benchmark structures and Buckminsterfullerene-like structures could be achieved with an excellent resolution (Figure 6).

Overall, the final order in printing efficiency for the studied PIs was BAPO < **1b** < **1a** < **2b** < **2a** (Table 3). Importantly, two trends are observed by linking the molecular structure to the photoinitiation efficiency in 2PLP. First, the printing of photoresists with the additional thiophenyl group in the exocyclic C=C of the pyran moiety (**2a** and **2b**) requires less irradiation dose than **1a** and **1b**. Second, additional phenyl groups in positions 2 and 6

Table 3. Results of 2PLP of benchmark structures in arrays with varying laser power and scanning speed.

Decreasing efficiency in 2PLP	Photoinitiator	c [μmol g^{-1}]	Minimum laser power for stable printed structures with 2 mm s^{-1} scanning speed [mW]
1	**2a**	37	10
2	**2b**	37	12
3	**1a**	37	22
4	**1b**	37	26
5	BAPO	320	–[a]
			30

[a] 2PLP was not possible with BAPO in a concentration lower than 100 μmol g^{-1}.[38]

of the pyranylidene ring in **1b** and **2b** reduce the 2PLP efficiency compared to their *tert*-butyl counterparts **1a** and **2a**. It is difficult to relate these results with the σ_{2PA} measurements: regarding the σ_{2PA} values at 780 nm (Figure 4b), higher σ_{2PA} values were encountered for **2** than **1**, but derivatives **b** show higher σ_{2PA} data than their analogs **a**. This is a clear indication that high σ_{2PA} is not the only criterion[1] affecting to the resolution/performance. That is, the ability of a 2PA PI eventually depends on a delicate balance between all the parameters participating in the process, mainly high σ_{2PA} and good radical generation ability among others. Thereby, the lower TPA for compounds of series **a** might be partly compensated by a possible better radical generation ability, as it has been reported for other π-conjugated PIs suitable for 2PLP.[42]

3. Conclusion

Four D–A–D systems featuring a 4*H*-pyranylidene donor moiety have been designed and synthesized, showing absorption maxima between 506 and 542 nm. Low fluorescence quantum yields were encountered, as desired for devising PIs, and in all cases, 2PA at 780 nm, the wavelength used for subsequent writing tests, was observed. The incorporation of a thiophene moiety in the exocyclic C=C bond of the pyranylidene unit leads to a hypsochromic shift of the absorption maxima, together with higher extinction coefficients, increased Stokes shifts and high 2PA cross section values, especially at 950 and 980 nm.

The 2PLP experiments performed to evaluate the photoinitiation ability of these systems in a pentaerythritol triacrylate resin formulation revealed higher efficiency, as compared to that of the commercially available BAPO: a lower concentration (until 3.3 times) and significantly lower laser powers were required for achieving stable microstructures. It is worth highlighting that the presence of a thiophene ring in the exocyclic C=C bond of the pyranylidene unit gave rise to the best initiation properties.

All these results render these chromophores especially promising as new 2PA photoinitiators.

4. Experimental Section

For General experimental methods, see Supporting Information.

Aldehydes **3a**,[30] **3b**,[31] **4a**[26] and compound **5**[31] were prepared as previously described. 4-methylcyclohexan-1-one and di(thiophen-2-yl)methanone (**6**) are commercially available.

5-((2,6-bis(4-(*tert*-butyl)phenyl)-4*H*-pyran-4-ylidene(thiophen-2-yl)methyl)thiophene-2-carbaldehyde **(4b)**

The tributyl phosphonium **5** (760 mg, 1.2 mmol) was dissolved in anhydrous THF (15 mL) under an argon atmosphere and cooled down to −78 °C. *n*-BuLi (1.6 M in hexanes) (0.53 mL, 1.33 mmol) was added dropwise to this solution, and the resulting mixture was stirred for 20 min. Ketone **6** (183 mg, 0.94 mmol) in anhydrous THF (8 mL) was then dropwise added, and the reaction crude was kept stirring at this temperature for an additional 20 min. Then, the reaction was progressively warmed up to r.t. and stirred overnight.

A saturated NH_4Cl solution was added to quench the reaction, then the desired product was extracted with CH_2Cl_2 (2 × 30 mL) and dried over anhydrous $MgSO_4$. The resulting solid was purified by column chromatography on silica gel with hexane/AcOEt (9.5:0.5) as eluent. An orange solid (474 mg, 96%) was obtained and identified by ^{1}H NMR (see below) as 2,6-bis(4-(*tert*-butyl)phenyl)-4-(di(thiophen-2-yl)methylene)-4*H*-pyran (**7**). It was used hereafter.

This solid was dissolved under an argon atmosphere in anhydrous 1,2-dichloroethane (13 mL) and anhydrous DMF (89 μL, 1.15 mmol) was added. The solution was cooled down to 0 °C and then, phosphorus oxychloride (101 μL, 1.08 mmol) was added dropwise. The reaction was stirred at 80 °C overnight. Then, it was slowly added under stirring over a saturated CH_3COONa solution for 20 min. The aqueous layer was extracted with AcOEt (3 × 25 mL) and dried over anhydrous $MgSO_4$. Afterward, the solvent was evaporated and the solid was purified by silica gel column chromatography (hexane/AcOEt 9.5:0.5). Yield: red oil (340 mg, 68% from compound **7**)

IR (KBr): $\bar{\nu}$ (cm^{-1}) = 2900, 2870 (O=C–H), 1650 (C=O), 1563, 1533, 1515 (C=C). ^{1}H NMR (300 MHz, CD_2Cl_2) δ (ppm) 9.82 (s, 1H), 7.76–7.72 (m, 2H), 7.69 (d, J = 4.0 Hz, 1H), 7.64–7.60 (m, 2H), 7.53–7.49 (m, 2H), 7.47–7.44 (m, 2H), 7.42 (dd, J = 5.2 Hz, J' = 1.2 Hz, 1H), 7.24 (d, J = 2.2 Hz, 1H), 7.12 (dd, J = 5.2 Hz, J' = 3.5 Hz, 1H), 7.08 (d, J = 4.0 Hz, 1H), 7.05 (d, J = 3.5 Hz, J' = 1.2 Hz, 1H), 6.70 (d, J = 2.2 Hz, 1H), 1.36 (s, 9H), 1.33 (s, 9H). ^{13}C NMR (75 MHz, CD_2Cl_2) δ (ppm) 182.8, 156.1, 154.9, 154.2, 154.0, 153.8, 143.6, 141.4, 137.3, 133.4, 130.5, 130.4, 128.7, 127.9, 127.8, 126.6, 126.4, 126.2, 125.5, 125.3, 109.3, 105.5, 104.1, 35.3, 35.2, 31.5, 31.4. HRMS (ESI$^+$): m/z calculated for $C_{35}H_{34}O_2S_2$ $M^{+\cdot}$ 550.1994; found 550.1974.

2,6-bis(4-(*tert*-butyl)phenyl)-4-(di(thiophen-2-yl)methylene)-4*H*-pyran (7)

^{1}H NMR (300 MHz, $CDCl_3$) δ (ppm) 7.66–7.63 (m, 2H), 7.46–7.43 (m, 2H), 7.30–7.28 (m, 1H), 7.06–7.03 (m, 2H), 6.90 (s, 1H), 1.35 (s, 9H).

(2*E*,6*E*)-2,6-bis((5-((2,6-di-*tert*-butyl-4*H*-pyran-4-ylidene)methyl)-thiophen-2-yl)methylene)-4-methylcyclohexan-1-one (**1a**)

To a suspension of 103 mg (0.326mmol) of aldehyde **3a** in EtOH (7 mL) under argon atmosphere, 4-methylcyclohexan-1-one (0.163 mmol) and aqueous NaOH 3.33 M (6.6 mg in 50 μL of water) were added. The mixture was stirred at 80 °C (TLC monitoring: Hexane/AcOEt 7:3) for 24 hours, adding after 3 h 30 min another portion of 4-methylcyclohexan-1-one and aqueous NaOH. Saturated NH_4Cl solution (20 mL) and 20 mL of chloroform were added, and the mixture was stirred for 10 min. Then, the organic layer was separated and washed with water (2 × 20 mL), dried over anhydrous $MgSO_4$, and evaporated. The resulting solid was washed with cool pentane, then a cool mixture of pentane/EtOH (9.5:0.5), finally with a cool mixture of pentane/CH_2Cl_2 (9.5:0.5), to afford **1a**, a garnet-brown solid (64 mg; 55%).

Mp (°C): 208–212. IR (KBr): $\bar{\nu}$ (cm^{-1}) = 1666 (C=O), 1582, 1560 (C=C). ^{1}H NMR (400 MHz, CD_2Cl_2) δ (ppm) 7.86 (d, J = 1.7 Hz, 2H), 7.26 (d, J = 4.0 Hz, 2H), 6.86 (d, J = 4.0 Hz, 2H), 6.55 (d, J = 1.5 Hz, 2H), 5.88 (s, 2H), 5.74 (d, J = 1.9 Hz, 2H), 3.23 (dd, J = 16.3 Hz, J' = 3.9 Hz, 2H), 2.48–2.40 (m, 2H), 2.04 (br s, 1H), 1.28 (s, 18H), 1.21–1.19 (m, 21H). ^{13}C NMR (75 MHz, CD_2Cl_2) δ (ppm) 166.3, 163.7, 148.8, 136.3, 134.1, 131.8, 131.0, 129.9, 125.3, 105.3, 104.8, 100.0, 37.1, 36.3, 35.8, 29.1, 28.1, 28.0, 22.2. HRMS (ESI$^+$): m/z calculated for $C_{45}H_{57}O_3S_2$ $(M + H)^+$ 709.3744; found 709.3744.

(2*E*,6*E*)-2,6-bis((5-((2,6-di-*tert*-butyl-4*H*-pyran-4-ylidene)(thiophen-2-yl) methyl)thiophen-2-yl)methylene)-4-methylcyclohexan-1-one (**2a**)

To a suspension of 100 mg (0.25 mmol) of aldehyde **4a** in EtOH (6 mL) under argon atmosphere 4-methylcyclohexan-1-one (0.125 mmol) and aqueous NaOH 3.33 M (5 mg in 37.5 μL of water) were added. The mixture was stirred at 80 °C (TLC monitoring: Hexane/AcOEt 8:2) for 6 h, adding after 2 h 30 min another portion of 4-methylcyclohexan-1-one and aqueous NaOH. Saturated NH_4Cl solution (20 mL) and 20 mL of chloroform were added, and the mixture was stirred for 10 min. Then, the organic layer was separated and washed with water (2 × 20 mL), dried over anhydrous $MgSO_4$, and evaporated. The resulting solid was washed with cool pentane, finally with a cool mixture of hexane/EtOH (9:1), to afford a garnet solid (51 mg; 47%).

Mp (°C): 210–218. IR (KBr): $\bar{\nu}$ (cm^{-1}) = 1664 (C=O), 1580, 1539, 1514 (C=C). ^{1}H NMR (300 MHz, CD_2Cl_2) δ (ppm) 7.85 (br s, 2H), 7.31 (dd, J = 5.2 Hz, J' = 1.1 Hz, 2H), 7.25 (d, J = 4.0 Hz, 2H), 7.05 (dd, J = 5.2 Hz, J' = 3.5 Hz, 2H), 6.92 (dd, J = 3.5 Hz, J' = 1.1 Hz, 2H), 6.85 (d, J = 3.9 Hz, 2H), 6.53 (d, J = 2.1 Hz, 2H), 6.01 (d, J = 2.1 Hz, 2H), 3.11 (dd, J = 16.5 Hz, J' = 3.8 Hz, 2H), 2.46–2.36 (m, 2H), 2.03 (br s, 1H), 1.22 (s, 18H), 1.16–1.15 (m, 21H). ^{13}C NMR (75 MHz, CD_2Cl_2) 188.3, 165.5, 164.8, 151.2, 144.6, 138.0, 133.8, 132.3, 131.8, 130.1, 127.7, 127.4, 127.4, 125.6, 107.3, 102.1, 101.3, 36.9, 36.2, 36.1, 29.0, 28.1, 28.1, 22.2. HRMS (ESI$^+$): m/z calculated for $C_{53}H_{61}O_3S_4$ $(M + H)^+$ 873.3498; found 873.3484.

(2*E*,6*E*)-2,6-bis((5-((2,6-bis(4-*tert*-butylphenyl)-4*H*-pyran-4-ylidene)-methyl)thiophen-2-yl))methylene)-4-methylcyclohexan-1-one (**1b**)

To a suspension of 155 mg (0.33 mmol) of aldehyde **3b** in EtOH (7 mL) under argon atmosphere 4-methylcyclohexan-1-one (0.165 mmol) and aqueous NaOH 3.33 M (6.6 mg in 50 μL of water) were added. The mixture was stirred at 80 °C (TLC monitoring: Hexane/AcOEt 7.5:2.5) for 48 h, adding after 3 and 24 h another portion of 4-methylcyclohexan-1-one and aqueous NaOH. Saturated NH_4Cl solution (20 mL) and 20 mL of chloroform were added, and the mixture was stirred for 10 min. Then, the organic layer was separated and washed with water (3 × 20 mL), dried over anhydrous $MgSO_4$, and evaporated. The resulting solid was washed with cool pentane, finally with a cool mixture of pentane/EtOH (9:1), to afford a dark brown solid (102 mg; 61%).

Mp (°C): 270–277. IR (KBr): $\bar{\nu}$ (cm^{-1}) 1655 (C=O), 1581, 1566, 1556 (C=C). ^{1}H NMR (400 MHz, CD_2Cl_2) δ (ppm) 7.91 (br s, 2H), 7.84–7.82 (m, 4H), 7.75–7.72 (m, 4H), 7.55–7.49 (m, 8H), 7.33 (d, J = 3.9 Hz, 2H), 7.27 (d, J = 1.6 Hz, 2H), 7.01 (d, J = 3.9 Hz, 2H), 6.49 (d, J = 1.6 Hz, 2H), 6.14 (s, 2H), 3.30 (dd, J = 15.8 Hz, J' = 3.5 Hz, 2H), 2.59–2.52 (m, 3H), 1.38–1.35 (m, 39H). ^{13}C NMR (75 MHz, CD_2Cl_2) δ (ppm) 187.9, 154.6, 153.9, 153.3, 152.3, 148.0, 137.2, 134.2, 131.6, 130.8, 130.6, 130.5, 129.9, 126.4, 126.3, 126.2, 125.4, 124.9, 108.4, 107.5, 102.9, 37.1, 35.3, 35.2, 31.5, 31.4, 29.1, 22.3. MS (MALDI$^+$): 1013.5 $(M + H)^+$.

(2*E*,6*E*)-2,6-bis((5-((2,6-bis(4-*tert*-butylphenyl)-4*H*-pyran-4-ylidene)-(thiophen-2-yl) methyl)thiophen-2-yl)methylene)-4-methylcyclohexan-1-one (**2b**).

To a suspension of 150 mg (0.27 mmol) of aldehyde **4b** in EtOH (10 mL) under argon atmosphere 4-methylcyclohexan-1-one (0.135 mmol) and aqueous NaOH 3.33 M (5.4 mg in 40.5 μL of water) were added. The mixture was stirred at 80 °C (TLC monitoring: Hexane/AcOEt 7:3) for 48 h, adding after 7, 24, and 30 h another portion of 4-methylcyclohexan-1-one and aqueous NaOH. Saturated NH_4Cl solution (20 mL) and 20 mL of chloroform were added, and the mixture was stirred for 10 min. Then, the organic layer was separated and washed with water (3 × 20 mL), dried over anhydrous $MgSO_4$, and evaporated. The resulting solid was washed with a cool mixture of pentane/EtOH (9.5:0.5), to afford a dark brown solid (91 mg; 57%).

Mp (°C): 250–255. IR (KBr): $\bar{\nu}$ (cm^{-1}) 1651 (C=O), 1580, 1537, 1517 (C=C). ^{1}H NMR (300 MHz, CD_2Cl_2) δ (ppm) 7.91 (br s, 2H), 7.74–7.70 (m, 4H), 7.65–7.62 (m, 4H), 7.50–7.44 (m, 8H), 7.39 (dd, J = 5.1 Hz, J' = 1.2 Hz, 2H), 7.34 (d, J = 4.0 Hz, 2H), 7.19 (d, J = 2.1 Hz, 2H), 7.11 (dd, J = 5.1 Hz, J' = 3.5 Hz, 2H), 7.07 (dd, J = 3.5 Hz, J' = 1.2 Hz, 2H), 7.04 (d, J = 3.9 Hz, 2H), 6.79 (d, J = 2.1 Hz, 2H), 3.14 (dd, J = 16.5 Hz, J' = 3.7 Hz, 2H), 2.52–2.43 (m, 2H), 2.03 (br s, 1H), 1.35 (s, 18H), 1.34 (s, 18H), 1.21 (d, J = 6.5 Hz, 3H). ^{13}C NMR (75 MHz, CD_2Cl_2) δ (ppm) 188.4, 154.0, 153.7, 153.5, 153.4, 150.7, 144.3, 139.0, 134.0, 132.3, 131.4, 130.8, 130.1, 128.2, 128.1, 127.6, 126.3, 126.2, 126.1, 125.3, 125.2, 110.1, 105.3, 104.5, 41.4, 35.4, 35.3, 31.5, 29.0, 22.2. HRMS (ESI$^+$): m/z calculated for $C_{77}H_{76}O_3S_4$ $M^{+\cdot}$ 1176.4672; found 1176.4709.

Supporting Information

Supporting Information is available from the Wiley Online Library or from the author.

Acknowledgements

Financial support from Ministerio de Ciencia e Innovación (PID2019-104307GB-I00/AEI/10.13039/501100011033 for Zaragoza group and PID2019-104293GB-I00 for F. Najera) and Gobierno de Aragón-FEDER-Fondo Social Europeo (E47_20R and E47_23R) is gratefully acknowledged. R.R. acknowledges the financial support of Gobierno de Aragón: Fellowship program 2018–2022 period co-financed with the Operational Program FSE Aragón 2014–2022. C.B.-M acknowledges Carl Tryggers Foundation for the Postdoctoral fellowship. E.B. acknowledges the funding from the Excellence Cluster "3D Matter Made to Order" (EXC-2082/1-390761711) and the Carl Zeiss Foundation through the "Carl-Zeiss-Foundation-Focus@HEiKA". The authors thank Dr. J. del Barrio (University of Zaragoza, Spain) for helpful discussions and Prof. Schröder (Heidelberg University) for the access to the electron microscopy facilities. The authors would like to acknowledge the use of Servicio General de Apoyo a la Investigación-SAI, Universidad de Zaragoza. The authors acknowledge the ICTS "NANBIOSIS" facilities, more specifically the U28 Unit of the Andalusian Centre for Nanomedicine & Biotechnology (BIONAND) where the 2PA characterization was carried out. The authors would like to thank the computer resources, technical expertise, and assistance provided by the SCBI (Supercomputing and Bioinformatics) Center of the University of Málaga.

Open access funding enabled and organized by Projekt DEAL.

Conflict of Interest

The authors declare no conflict of interest.

Data Availability Statement

The data that support the findings of this study are available from the corresponding author upon reasonable request.

Keywords

3D nanoprinting, 4*H*-pyranylidene, photopolymerization, two-photon absorption, two-photon laser printing

Received: April 13, 2023
Revised: May 9, 2023
Published online:

[1] S. C. Ligon, R. Liska, J. Stampfl, M. Gurr, R. Mülhaupt, *Chem. Rev.* **2017**, *117*, 10212.
[2] D. Gräfe, S. L. Walden, J. Blinco, M. Wegener, E. Blasco, C. Barner-Kowollik, *Angew. Chem., Int. Ed.* **2020**, *59*, 6330.
[3] M. Pawlicki, H. A. Collins, R. G. Denning, H. L. Anderson, *Angew. Chem., Int. Ed.* **2009**, *48*, 3244.

[4] J.-F. Xing, W.-Q. Chen, X.-Z. Dong, T. Tanaka, X.-Y. Fang, X.-M. Duan, S. Kawata, *J. Photochem. Photobiol. A* **2007**, *189*, 398.
[5] Q. Zou, Y. Zhao, N. S. Makarov, J. Campo, H. Yuan, D.-C. Fang, J. W. Perry, F. Wu, *Phys. Chem. Chem. Phys.* **2012**, *14*, 11743.
[6] M.-L. Zheng, X.-M Duan, *Multiphoton Lithography: Techniques, Materials and Applications*, Wiley-VCH, Weinheim, Germany, **2016**.
[7] T. Wloka, M. Gottschaldt, U. S. Schubert, *Chem. - Eur. J.* **2022**, *28*, e202104191.
[8] G. S. He, L.-S. Tan, Q. Zheng, P. N. Prasad, *Chem. Rev.* **2008**, *108*, 1245.
[9] Z. Li, N. Pucher, K. Cicha, J. Torgersen, S. C. Ligon, A. Ajami, W. Husinsky, A. Rosspeintner, E. Vauthey, S. Naumov, T. Scherzer, J. Stampfl, R. Liska, *Macromolecules* **2013**, *46*, 352.
[10] G. Lemercier, C. Martineau, J.-C. Mulatier, I. Wang, O. Stéphan, P. Baldeck, C. Andraud, *New J. Chem.* **2006**, *30*, 1606.
[11] P. Hu, J. Zhu, R. Liu, Z. Li, *J. Photopolym. Sci. Technol.* **2019**, *32*, 257.
[12] B. H. Cumpston, S. P. Ananthavel, S. Barlow, D. L. Dyer, J. E. Ehrlich, L. L. Erskine, A. A. Heikal, S. M. Kuebler, I.-Y. S. Lee, D. McCord-Maughon, J. Qin, H. Röckel, M. Rumi, X.-L. Wu, S. R. Marder, J. W. Perry, *Nature* **1999**, *398*, 51.
[13] W. Qiu, P. Hu, J. Zhu, R. Liu, Z. Li, Z. Hu, Q. Chen, K. Dietliker, R. Liska, *ChemPhotoChem* **2019**, *3*, 1090.
[14] I. Henning, A. W. Woodward, G. A. Rance, B. T. Paul, R. D. Wildman, D. J. Irvine, J. C. Moore, *Adv. Funct. Mater.* **2020**, *30*, 2006108.
[15] X. Wang, F. Jin, Z. Chen, S. Liu, X. Wang, X. Duan, X. Tao, M. Jiang, *J. Phys. Chem. C* **2011**, *115*, 776.
[16] B. Holzer, M. Lunzer, A. Rosspeintner, G. Licari, M. Tromayer, S. Naumov, D. Lumpi, E. Horkel, C. Hametner, A. Ovsianikov, R. Liska, E. Vauthey, J. Fröhlich, *Mol. Syst. Des. Eng.* **2019**, *4*, 437.
[17] Z. Li, M. Siklos, N. Pucher, K. Cicha, A. Ajami, W. Husinsky, A. Rosspeintner, E. Vauthey, G. Gescheidt, J. Stampfl, R. Liska, *J. Polym. Sci., Part A: Polym. Chem.* **2011**, *49*, 3688.
[18] B. S. Haq, H. U. Khan, K. Alam, S. Attaullah, I. Zari, M. Mateenullah, *Appl. Opt.* **2015**, *54*, 7020.
[19] M. Tromayer, P. Gruber, A. Rosspeintner, A. Ajami, W. Husinsky, F. Plasser, L. González, E. Vauthey, A. Ovsianikov, R. Liska, *Sci. Rep.* **2018**, *8*, 17273.
[20] R. Andreu, L. Carrasquer, S. Franco, J. Garín, J. Orduna, N. Martínez de Baroja, R. Alicante, B. Villacampa, M. Allain, *J. Org. Chem.* **2009**, *74*, 6647.
[21] R. J. Durand, S. Gauthier, S. Achelle, T. Groizard, S. Kahlal, J.-Y. Saillard, A. Barsella, N. Le Poul, F. Robin-Le Guen, *Dalton Trans.* **2018**, *47*, 3965.
[22] S. Gauthier, F. Robin-Le Guen, L. Wojcik, N. Le Poul, A. Planchat, Y. Pellegrin, P. Guevara Level, N. Szuwarski, M. Boujtita, D. Jacquemin, F. Odobel, *Dyes Pigm.* **2019**, *171*, 107747.
[23] R. Andreu, E. Galán, J. Orduna, B. Villacampa, R. Alicante, J. T. López Navarrete, J. Casado, J. Garín, *Chem. - Eur. J.* **2011**, *17*, 826.
[24] C. Moreno-Yruela, J. Garín, J. Orduna, S. Franco, E. Quintero, J. T. López Navarrete, B. E. Diosdado, B. Villacampa, J. Casado, R. Andreu, *J. Org. Chem.* **2015**, *80*, 12115.
[25] A. B. Marco, N. Martínez de Baroja, J. M. Andrés-Castán, S. Franco, R. Andreu, B. Villacampa, J. Orduna, J. Garín, *Dyes Pigm.* **2019**, *161*, 205.
[26] J.-M. Andrés-Castán, R. Andreu, B. Villacampa, J. Orduna, S. Franco, *Sol. Energy* **2019**, *193*, 74.
[27] Y. M. Poronik, V. Hugues, M. Blanchard-Desce, D. T. Gryko, *Chem. - Eur. J.* **2012**, *18*, 9258.
[28] S. Gámez-Valenzuela, D. Neusser, C. Benitez-Martin, F. Najera, J. A. Guadix, C. Moreno-Yruela, B. Villacampa, R. Ponc Ortiz, S. Ludwigs, R. Andreu, M. C. Ruiz Delgado, *Mater. Adv.* **2021**, *2*, 4255.
[29] A. R. Morales, A. Frazer, A. W. Woodward, H.-Y. Ahn-White, A. Fonari, P. Tongwa, T. Timofeeva, K. D. Belfield, *J. Org. Chem.* **2013**, *78*, 1014.
[30] S. Franco, J. Garín, N. Martínez de Baroja, R. Pérez-Tejada, J. Orduna, Y. Yu, M. Lira-Cantú, *Org. Lett.* **2012**, *14*, 752.
[31] J. M. Andrés-Castán, S. Franco, B. Villacampa, J. Orduna, R. Pérez-Tejada, *RSC Adv.* **2015**, *5*, 106706.
[32] V. Tejeda-Orusco, M. Blais, C. Cabanetos, P. Blanchard, R. Andreu, S. Franco, J. Orduna, B. E. Diosdado, *Dyes Pigm.* **2020**, *178*, 108357.
[33] V. Tejeda-Orusco, R. Andreu, J. Orduna, B. Villacampa, S. Franco, A. Civera, *J. Org. Chem.* **2021**, *86*, 3152.
[34] V. F. Pais, P. Ramírez-López, A. Romero-Arenas, D. Collado, F. Najera, E. Pérez-Inestrosa, R. Fernández, J. M. Lassaletta, A. Ros, U. Pischel, *J. Org. Chem.* **2016**, *81*, 9605.
[35] F. Terenziani, C. Katan, E. Badaeva, S. Tretiak, M. Blanchard-Desce, *Adv. Mater.* **2008**, *20*, 4641.
[36] C. Benitez-Martin, B. Donoso, I. Torres-Moya, J. Herrera, A. Díaz-Ortiz, F. Najera, P. Prieto, E. Perez-Inestrosa, *Dyes Pigm.* **2022**, *200*, 110149.
[37] S.-J. Chung, S. Zheng, T. Odani, L. Beverina, J. Fu, L. A. Padilha, A. Biesso, J. M. Hales, X. Zhan, K. Schmidt, A. Ye, E. Zojer, S. Barlow, D. J. Hagan, E. W. Van Stryland, Y. Yi, Z. Shuai, G. A. Pagani, J.-L. Brédas, J. W. Perry, S. R. Marder, *J. Am. Chem. Soc.* **2006**, *128*, 14444.
[38] M. Lunzer, J. S. Beckwith, F. Chalupa-Gantner, A. Rosspeintner, G. Licari, W. Steiger, C. Hametner, R. Liska, J. Fröhlich, E. Vauthey, A. Ovsianikov, B. Holzer, *Chem. Mater.* **2022**, *34*, 3042.
[39] N. Silbernagel, A. Körner, J. Balitzki, M. Jaggy, S. Bertels, B. Richter, M. Hippler, A. Hellwig, M. Hecker, M. Bastmeyer, N. D. Ullrich, *Biomaterials* **2020**, *227*, 119551.
[40] L.-Y. Hsu, P. Mainik, A. Münchinger, S. Lindenthal, T. Spratte, A. Welle, J. Zaumseil, C. Selhuber-Unkel, M. Wegener, E. Blasco, *Adv. Mater. Technol.* **2023**, *8*, 2200801.
[41] M. del Pozo, C. Delaney, C. W. M. Bastiaansen, D. Diamond, A. P. H. J. Schenning, L. Florea, *ACS Nano* **2020**, *14*, 9832.
[42] C. Arnoux, T. Konishi, E. van Elslande, E.-A. Poutougnigni, J.-C. Mulatier, L. Khrouz, C. Bucher, E. Dumont, K. Kamada, C. Andraud, P. Baldeck, A. Banyasz, C. Monnereau, *Macromolecules* **2020**, *53*, 9264.